Volume 1 | Number 1 | Jan 2013 | Pages 1–100

ChemComm

Chemical Communications
www.rsc.org/chemcomm

ROYAL SOCIETY OF CHEMISTRY

ROYAL SOCIETY OF CHEMISTRY

www.rsc.org/chemcomm

ChemComm

COMMUNICATION

DNA polygonal cavities with tunable shapes and sizes†

Sha Sun, Mingyang Wang, Feifei Zhang and Jin Zhu*

We developed a new and simple angle control strategy to construct shape- and size-tunable DNA polygonal cavities. A monomer with a controlled slope on one end was used for hierarchical assembly into diverse polygons in a single step. Additionally, by simply moving the position of sticky ends on the monomer, the cavity size can be precisely programmed.

Cavities with diverse shapes and sizes in inorganic and organic structures (e.g., molecular sieves and enzymes) have shown exquisite control over the reaction selectivity and specificity in catalytic chemistry and biology,[1] as well as the processes of cellular uptake and biodistribution as drug carriers.[2] As a promising approach, DNA nanotechnology offers an opportunity to construct complex geometries with high precision and tunability. To date, diverse cavities have been constructed by DNA origami.[3] However, this strategy not only suffers from limitations on the dimension of target structure (dictated by the length of scaffold DNA), but also requires a new design and a new set of staple DNA sequences for each structure. A promising route to overcoming these two problems is the hierarchical assembly,[4] in which a basic building block (monomer) constructed first with unique DNA strands is used to assmeble into larger structures and minor changes of the monomer results in the alteration of the target structure. When aiming for the large hollow nanostructures, n-arm-junction (arm is used as a unit to form a junction) motif[4] is typically used as the monomer. This strategy is well suited for the structure fabrication by small molecular weight monomers (<170 kD),[4a-d] with the target morphology controlled by the flexibility and concentration of the monomer. However, it is much more challenging for the large, magadaltons monomer, in which the fixation of the inter-arm angle is required for the construction of target structures.[4e] Herein we report a general

strategy to assemble large monomers (~1.5 MD) into target structures, with polygonal cavities as the proof-of-concept system.
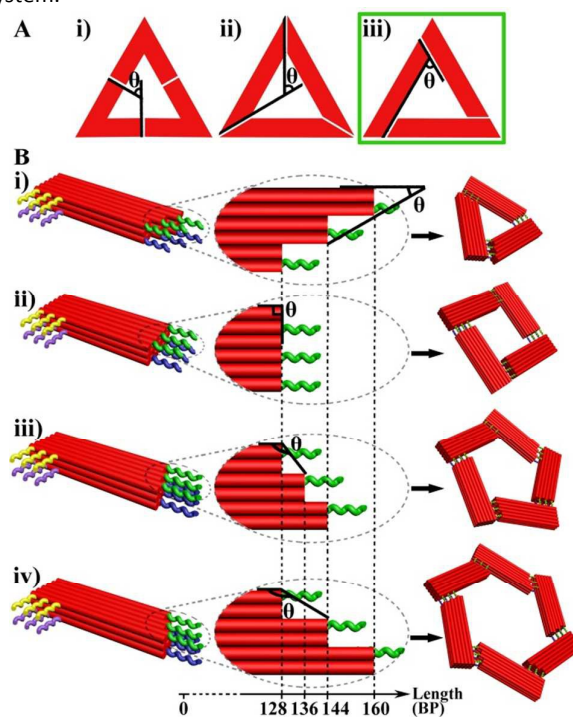

Fig. 1 (A) Three hierarchical assembly strategies with different angle control principles. (B) Schematic illustration of self-assembled polygons. The helical length difference △L of the monomer controls the angle θ. The middle column shows zoomed-in images of the first layer of the monomers (with sticky ends shown in green) in the left column. Polygons (right column) are assembled by the hybridization of the sticky ends between the monomers: i) triangle, ii) square, iii) pentagon, iv) hexagon.

In geometry, the shape of a physical object is defined by the relative positions of vertices,[5] which are dictated by internal angles. Therefore, the key to the construction of shape-tunable cavities is the control over angles. To achieve the hierarchical assembly of target geometric cavities, three strategies with different angle control principles can be

Department of Polymer Science and Engineering, School of Chemistry and Chemical Engineering, State Key Laboratory of Coordination Chemistry, Nanjing National Laboratory of Microstructures, Collaborative Innovation Center of Chemistry for Life Sciences, Nanjing University, Nanjing 210093, China. E-mail: jinz@nju.edu.cn

COMMUNICATION

ChemComm

imagined (Fig. 1A). In each monomer, the angle θ between two monomer connection sites equals the value of the interior angle and hence controls the shape of the target structure. Among the three strategies, the monomer in strategy i, consisted of two arms with a controlled angle, requires a much more complex structure than that in strategy ii or iii with one arm for each monomer. For strategies i and ii, θ can be tuned by adjusting the inter-arm angle, as typically used previously[4e] but with a complex design required (strategy i), or by adjusting the slopes of both ends in the monomer (strategy ii). Compared to the complicated angle control methods in the first two strategies, strategy iii features a simpler approach in which θ can be tuned by adjusting the slope of only one end of the monomer. In addition, because one of the connection sites lies on the inner edge instead of the end, strategy iii offers a straightforward route to tuning the cavity size by simply moving the connection site in the longitudinal direction, instead of the tedious way of altering the dimension of the monomer as required by the first two strategies.

Herein, we use strategy iii to hierarchically construct shape- and size-tunable polygonal cavities. As Fig. 1B shows, monomers constructed by single-stranded DNA (ssDNA) could assemble into polygons without intermediate purification by the hybridization between sticky ends on the tail (Sticky End 1, comprised of three green strands and three blue strands) and the sticky ends on the inner surface (Sticky End 2, comprised of three yellow strands and three purple strands). Diverse polygons can be constructed by monomers with different angle θ. Helices of the monomer are divided into three categories: six outer helices (with the length of L_{outer}, 6H (helices) = 2H/layer × 3 layers,), six middle helices (with the length of L_{middle}), and six inner helices (with the length of L_{inner}). The helical length difference ($\triangle L = L_{outer} - L_{milldle} = L_{middle} - L_{inner}$) between adjacent categories of helices controls angle θ. In addition, the cavity size, with the side length corresponding to the distance between Sticky End 2 and the tail of the monomer, can be readily controlled by changing the location of Sticky End 2 along the helical axis. Furthermore, the strategy for constructing two-dimensional (2D) polygons can in principle be extended to three-dimensional (3D) wire-frame structures (mirroring the development from relatively open 2D cavity[6a] to relatively closed 3D cavity structures[6b] in supramolecular chemistry) by the hierarchical assembly of L-shaped monomers, in which one arm resembling the monomer of the polygonal cavity described above serves as the polygonal base edge and the other arm with a cuboid shape serves as half of the lateral edge (schematic illustration in Fig. S7, ESI†).

The ssDNA bricks strategy[7a] developed previously has proved to be a powerful method to fabricate 3D structures. The greatest advantage of this method is that arbitrary structures can be sculpted from the predesigned 3D molecular canvas, making the design process easier and more straightforward. Therefore, helical lengths can be adjusted by adding or deleting a part of short ssDNA sequences from a DNA pool and most of the sequences are reusable for different monomers. We name the monomers (Fig. 1B, left column) without sticky ends Monomer A (Fig. 1B, i), Monomer B (Fig.

1B, ii), Monomer C (Fig. 1B, iii) and Monomer D (Fig. 1B, iv), respectively. Accordingly, polygons (Fig. 1B, right column) constructed by the monomers are named A0 (Fig. 1B, i), B0 (Fig. 1B, ii), C0 (Fig. 1B, iii) and D0 (Fig. 1B, iv). For Monomer A, L_{outer}, $L_{middler}$ and L_{inner} are 160BP (base pairs), 144BP and 128BP, respectively, with $\triangle L$ of 16BP and θ of 43° (assuming 0.34 nm for per base pair and 2.5 nm for the diameter of a DNA helix). For Monomer B, all the 18 helices share the equal length of 128BP, leading to $\triangle L$ of 0BP and θ of 90°. For Monomer C, L_{outer}, $L_{middler}$ and L_{inner} are 128BP, 136BP and 144BP, respectively, with $\triangle L$ of -8BP and θ of 118°. For Monomer D, L_{outer}, $L_{middler}$ and L_{inner} are 128BP, 144BP and 160BP, respectively, with $\triangle L$ of -16BP and θ of 137°. It is noted that Monomer A can be obtained by rotating Monomer D 180° along the helical axis, indicating that only Monomer D is needed for the construction of both the triangle and the hexagon.
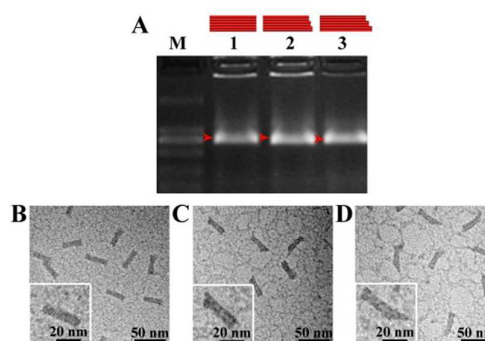

Fig. 2 DNA self-assembly for the fabrication of monomers. (A) Agarose gel electrophoresis of Monomer B (lane 1), Monomer C (lane 2) and Monomer D (lane 3). Lane M represents molecular weight marker DL 2000. The product bands are marked with red arrowheads. TEM images of Monomer B (B), Monomer C (C) and Monomer D (D). The insets are zoomed-in views.

First, we constructed and characterized three types of monomers: Monomer B, Monomer C and Monomer D. Monomers were assembled by slow annealing of hundreds of ssDNA sequences from 90 °C to 61 °C at a cooling rate of 5 min/°C and 60 °C to 24 °C at a rate of 40 min/°C. Agarose gel electrophoresis revealed a dominant band for each monomer (Fig. 2A). By using fluorescence intensity as the quantification tool,[7] we obtained the assembly yields of 67.1%, 75.0% and 74.1% for Monomer B, Monomer C and Monomer D, respectively. To confirm their correct formation, unpurified samples stained by uranyl formate were imaged with transmission electron microscopy (TEM).[8] TEM images (Fig. 2B, C, D) showed that the tail slope of the monomer increased with the increase of the designed θ from Monomer B to Monomer D. Statistically, θ were measured as 87 ± 5°, 110 ± 3°and 136 ± 5° for Monomer B, Monomer C and Monomer D, respectively, consistent with the designed values.

We next verified the working principle of hierarchical self-assembly by constructing polygons with the monomers. By replacing corresponding strands in the DNA pool for the monomer, two sets of sticky ends (Sticky End 1 and Sticky End 2) are added to the monomer, enabling the association of

monomers to construct a polygon. Sticky End 1 is anchored on the tail of the monomer with three green strands on the first layer and three blue strands on the third layer (Fig. 1B, left column). It has been demonstrated that protruded continuous thymidines on both ends of all the helices are essential for the assembly of DNA nanostructures to prevent unwanted aggregation from blunt-end stacking.[3a,7] In our design, T16 (sixteen thymidines) loops are added to the head of the monomer and T8 (eight thymidines) single strands are added to the tail. Sticky End 1 anchored on the tail of the monomer is covalently linked to T8 of six corresponding helices. In addition, T8 linked to Sticky End 1 could serve as a linker to allow two sets of sticky ends to encounter each other and hybridize more effectively for the construction of a closed structure by increasing the flexibility of Sticky End 1.

Accordingly, Sticky End 2 is anchored on the inner surface of the monomer. Three yellow strands on the first layer are located close to the head with the interval of 16BP, the positions of which are identical to those of three purple strands on the third layer (Fig. 1B, left column). It is noted that for a polygon with larger size than a square, such as a pentagon or a hexagon, the inner surface of the monomer refers to the surface with longer helical length. However, it is opposite for a polygon with smaller size than a square: the triangle—the smallest polygon, of which the surface with shorter helical length is the inner surface. Therefore, for the construction of the pentagon and the hexagon, Sticky End 2 should be anchored to the surface with longer helical length of Monomer C and Monomer D, respectively. On the contrary, the triangle is designed to be constructed by Monomer D with Sticky End 2 added to the surface with shorter helical length. Monomer B, in which all the helices share the equal length, is expected to assemble into the square by adding Sticky End 2 to either of the surfaces.

By annealing the mixed ssDNA sequences slowly, monomers were first assembled and then associated with each other by sticky ends to form a polygon. Annealed samples were subjected to the agarose gel electrophoresis and a sharp band was observed for each structure (Fig. 3A). The band moving slower than the product in lane 1 corresponds to the dimer of A0 with the yield of 15.1%, comparable with the yield of 20.1% for A0. Assembly yields estimated from the gel for B0, C0 and D0 were 34.8%, 24.7% and 14.2%, respectively. TEM imaging showed uniform-sized and closed polygonal structures as expected (A0, Fig. 3B; B0, Fig. 3C; C0, Fig. 3D; D0, Fig. 3E), suggesting the successful implementation of our strategy (TEM yields for all the structures are shown in Table 1, ESI†).

We note that the assembly yield decreases as the size of the polygonal structure increases. This phenomenon might be explained by the fact that more monomers are required for the construction of larger structures which thus are more difficult to assemble.[4d] When constructing the desired structure by the monomer with controlled angle, another factor should be taken into consideration: kinetics. It has been experimentally demonstrated that smaller-size object is kinetically favored.[4e] Therefore, with the T8 linkers increasing the flexibility, Monomer C (with the designed θ of 118°) favors

the assembly into pentagon instead of hexagon and Monomer D (with the designed θ of 137°) favors hexagon instead of octagon.
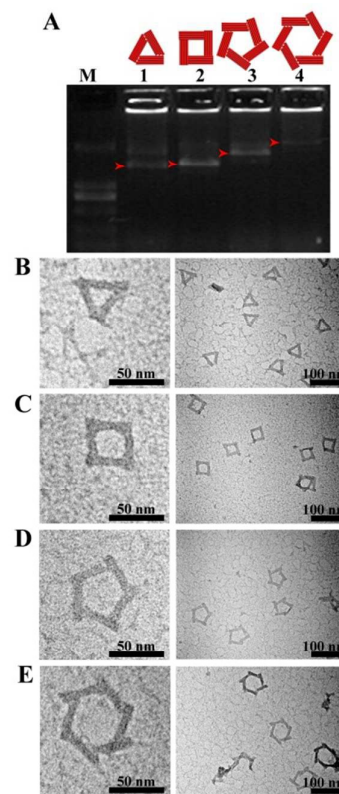

Fig. 3 Polygons formed from DNA monomer self-assembly. (A) Agarose gel electrophoresis of A0 (lane 1), B0 (lane 2), C0 (lane 3) and D0 (lane 4). The product bands are marked with red arrowheads. TEM images of A0 (B), B0 (C), C0 (D) and D0 (E). The left images are zoomed-in views.

Based on the successful assembly of diverse polygonal cavities, we further tuned the cavity size by adjusting the location of Sticky End 2 attached on the monomer, with decreased distance between Sticky End 2 and the tail decreasing the cavity size. Herein, with Sticky End 1 fixed on the tail of the monomer, we move Sticky End 2 from the head to the tail along the helical axis with the interval of 16BP (corresponding to 5.4 nm), which results in polygonal cavities with a variety of sizes (location details are provided in Fig. S3 to S6, ESI†). Four types of polygonal structures described above were tested, with four different cavity sizes for each structure (Fig. 4). As the side length of the cavity decreased, the length of the branch extended out from the cavity increased accordingly. The triangular cavities (Fig. 4, A1 to A4) and square cavities (Fig. 4, B1 to B4), as verified by TEM imaging, showed desired morphologies. In the construction of pentagonal cavities (Fig. 4, C1 to C4), expected structures were observed for C1, C2 and C4. Interestingly, stacked structure (instead of individual structure), which is formed by two desired structures with mirror symmetry, was observed for C3 (for stacking mechanism, see Fig. S15, ESI†). A similar phenomenon occurs for the hexagonal cavities (Fig. 4, D1 to

COMMUNICATION

D4; for stacking mechanism of D3, see Fig. S18, ESI†). We measured the side lengths of A0 to D0 and all the cavities in Fig. 4 (Data are provided in Fig. S10, S12, S14, and S17, ESI†). As Fig. 4E showed, the side length decreases in a linear fashion for each group, consistent with the designed interval of 5.4 nm.
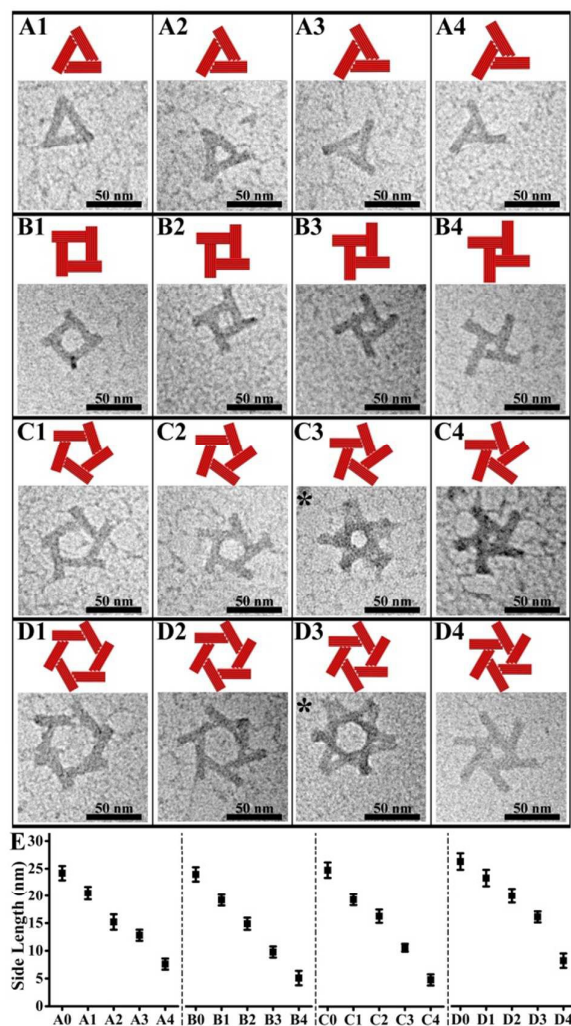
Fig. 4 Tuning of polygonal cavity sizes. (A1 to A4) Triangular cavities. (B1 to B4) Square cavities. (C1 to C4) Pentagonal cavities. (D1 to D4) Hexagonal cavities. (E) Side lengths measured for cavities with different shapes and sizes. C3 and D3 marked with * show stacked structures of desired products.

In conclusion, we have developed a simple and general angle control strategy to hierarchically assemble shape- and size-tunable polygonal cavities. With a monomer bearing a controlled slope on one end, polygons can be constructed, with the cavity size precisely programmable by the adjustment of the sticky end position. In addition to the expected utilization in the construction of 3D polyhedral structures, our strategy shows great potential in the construction of complex nanocontainers for the application in drug delivery,[9] material organization[10] and molecular reactors.[11]

References

1   (a) U. Olsbye, S. Svelle, M. Bjørgen, P. Beato, T. V. Janssens, F. Joensen and K. P. Lillerud, *Angew. Chem. Int. Ed.*, 2012, **51**, 5810-5831; (b) N. R. Shiju and V. V. Guliants, *Appl. Catal. A: Gen.*, 2009, **356**, 1-17; (c) T. S. Koblenz, J. Wassenaar and J. N. Reek, *Chem. Soc. Rev.*, 2008, **37**, 247-262; (d) M. Stahl, C. Taroni and G. Schneider, *Protein Eng.*, 2000, **13**, 83-88; (e) J. Liang, C. Woodward and H. Edelsbrunner, *Protein Sci.*, 1998, **7**, 1884-1897.
2   (a) S. Venkataraman, J. L. Hedrick, Z. Y. Ong, C. Yang, P. L. R. Ee, P. T. Hammond and Y. Y. Yang, *Adv. Drug Deliv. Rev.*, 2011, **63**, 1228-1246; (b) J. A. Champion and S. Mitragotri, *Proc. Natl. Acad. Sci. USA*, 2006, **103**, 4930-4934.
3   (a) P. W. K. Rothemund, *Nature*, 2006, **440**, 297–302; (b) E. S. Andersen, M. Dong, M. M. Nielsen, K. Jahn, R. Subramani, W. Mamdouh, M. M. Golas, B. Sander, H. Stark, C. L. Oliveira, J. S. Pedersen, V. Birkedal, F. Besenbacher, K. V. Gothelf and J. Kjems, *Nature*, 2009, **459**, 73-76; (c) Y. Ke, J. Sharma, M. Liu, K. Jahn, Y. Liu and H. Yan, *Nano Lett.*, 2009, **9**, 2445-2447; (d) M. Endo, K. Hidaka, T. Kato, K. Namba and H. Sugiyama, *J. Am. Chem. Soc.*, 2009, **131**, 15570-15571; (e) D. M. Smith, V. Schüller, C. Forthmann, R. Schreiber, P. Tinnefeld and T. Liedl, *J. Nucleic Acids*, 2011, **2011**, 360954-360962; (f) W. M. Shih, J. D. Quispe and G. F. Joyce, *Nature*, 2004, **427**, 618-621; (g) D. Han, S. Pal, J. Nangreave, Z. Deng, Y. Liu and H. Yan, *Science*, 2011, **332**, 342-346.
4   (a) Y. He, Y. Chen, H. Liu, A. E. Ribbe and C. Mao, *J. Am. Chem. Soc.*, 2005, **127**, 12202-12203; (b) C. Zhang, S. H. Ko, M. Su, Y. Leng, A. E. Ribbe, W. Jiang and C. Mao, *J. Am. Chem. Soc.*, 2009, **131**, 1413-1415; (c) C. Zhang, M. Su, Y. He, X. Zhao, P. Fang, A. E. Ribbe, W. Jiang and C. Mao, *Proc. Natl. Acad. Sci. USA*, 2008, **105**, 10665–10669; (d) Y. He, T. Ye, M. Su, C. Zhang, A. E. Ribbe, W. Jiang and C. Mao, *Nature*, 2008, **452**, 198–201; (e) R. Iinuma, Y. Ke, R. Jungmann, T. Schlichthaerle, J. B. Woehrstein and P. Yin, *Science*, 2014, **344**, 65-69.
5   D. G. Kendall, *B. Lond. Math. Soc.*, 1984, **16**, 81-121.
6   (a) R. M. Izatt, J. S. Bradshaw, S. A. Nielsen, J. D. Lamb and J. J. Christensen, *Chem. Rev.*, 1985, **85**, 271-339; (b) C. Seel and F. Vögtle, *Angew. Chem. Int. Ed.*, 1992, **31**, 528-549.
7   (a) Y. Ke, L. L. Ong, W. M. Shih and P. Yin, *Science*, 2012, **338**, 1177-1183; (b) B. Wei, M. Dai and P. Yin, *Nature*, 2012, **485**, 623–626.
8   S. Sun, H. Yao, F. Zhang and J. Zhu, *Chem. Sci.*, 2015, **6**, 930-934.
9   (a) A. S. Walsh, H. Yin, C. M. Erben, M. J. Wood and A. J. Turberfield, *ACS Nano*, 2011, **5**, 5427-5432; (b) Q. Jiang, C. Song, J. Nangreave, X. Liu, L. Lin, D. Qiu and B. Ding, *J. Am. Chem. Soc.*, 2012, **134**, 13396-13403; (c) S. M. Douglas, I. Bacheleta and G. M. Church, *Science*, 2012, **335**, 831-834.
10   (a) Z. Zhao, E. L. Jacovetty, Y. Liu and H. Yan, *Angew. Chem. Int. Ed.*, 2011, **50**, 2041-2044; (b) W. Shen, H. Zhong, D. Neff, M. L. Norton, *J. Am. Chem. Soc.*, 2009, **131**, 6660–6661; (c) H. Bui, C. Onodera, C. Kidwell, Y. Tan, E. Graugnard, W. Kuang and W. L. Hughes, *Nano Lett.*, 2010, **10**, 3367-3372; (d) J. Sharma, R. Chhabra, A. Cheng, J. Brownell, Y. Liu and H. Yan, *Science*, 2009, **323**, 112-116.
11   (a) M. Liu, J. Fu, C. Hejesen, Y. Yang, N. W. Woodbury, K. Gothelf and H. Yan, *Nat. Commun.*, 2013, **4**, 2127-2131; (b) O. I. Wilner, Y. Weizmann, R. Gill, O. Lioubashevski, R. Freeman and I. Willner, *Nat. Nanotechnol.*, 2009, **4**, 249-254; (c) T. Douglas and M. Young, *Nature*, 1998, **393**, 152-155.

ChemComm Accepted Manuscript